Turkish Journal of Electromechanics & Energy
ISSN: 2547-975X
Vol:9, No:2, Page 76-84 (2024)
https://www.scienceliterature.com

Design and development of a VTOL UAV arm for heavy load lifting

F. Akkoyun[1, *], İ. Böğrekci[2]

[1]Department of Mechanical Engineering, İzmir Demokrasi University, İzmir, 35040, Türkiye

[2]Department of Mechanical Engineering, Aydın Adnan Menderes University, Aydın, 09010, Türkiye

ARTICLE INFO

***Article Type*:**
Research Article

Article History:
Received: 22 August 2024
Revised: 19 September 2024
Accepted: 23 September 2024
Published: 15 October 2024

Editor of the Article:
M. E. Şahin

Keywords:
VTOL UAV arm, Propeller thrust, Arm characterization, Propeller thrust measurement

ABSTRACT

Mid-size unmanned aerial vehicles (UAVs), have gained popularity recently for civil applications including agricultural spraying and transportation. These applications require larger propellers and higher power to handle heavier payloads. Medium-sized UAVs are becoming more and more crucial to achieving all transportation objectives. For this reason, carbon fibre frames are frequently employed in constructing widely used UAVs due to their ease of assembly and availability in markets. However, these UAV frames are expensive and have limited manufacturing capacity. The present study aimed to develop a Mid-Size UAV arm that is suitable for rapid manufacturing by using common manufacturing techniques. In line with this purpose, a vertical take-off and landing (VTOL) UAV arm was designed, analysed, and developed. The parameters of displacement, safety factor, stress (σ), and strain (ε) were compared between experimental test results and computer-based structural analysis results. To investigate the relationship between thrust force and strain, an experimental test was accomplished with the help of a UAV arm testing mechanism. The developed arm of the UAV is capable of producing thrust up to 250 N at about 5000 rpm using a 6.5 kW power brushless direct current motor and the reducer.

Cite this article: F. Akkoyun, İ. Böğrekçi, "Design and development of a VTOL UAV arm for heavy load lifting," *Turkish Journal of Electromechanics & Energy*, 9(2), pp.76-84, 2024.

1. INTRODUCTION

Unmanned aircraft systems (UAS) term is used to define a system, which comprises an unmanned flying aircraft with the guidance of a base station for supervising the aerial vehicle in a mission [1]. The unmanned aerial vehicle (UAV) is the most significant part of the UAS, in the early years it was also known as a drone, states for a pilotless aircraft that flies without the intervention of a pilot. It can be either remotely controlled, named remotely piloted vehicle (RPV), or it can fly autonomously for a specific mission [2-4]. Typically, the flights are remotely monitored and controlled by a ground control system (GCS). However, the vehicle should be under the control of the pilot at flying time for safety reasons [5-6]. The term UAV encompasses various types, including fixed-wing and rotary-wing UAVs, lighter-than-air UAVs, lethal aerial vehicles, decoys and targets, alternatively piloted aircraft, and uninhabited combat aerial vehicles [5]. Many applications can be done with the help of a UAV, including defence, farming, and remote sensing [2]. Unmanned aerial vehicles (UAVs) equipped with vision sensors are capable of a range of monitoring duties, including remote sensing, traffic surveillance, forest protection, reconnaissance, remote mapping, and search and rescue missions [6]. UAVs have a wide range of applications for military-based applications and in civilian scenarios [7]. Based on flying altitude and endurance limitations, six major categories of UAS platforms can be distinguished. These kinds of UAS are, Nano- or micro-air vehicles, or MAVs; Take-off and landing vertically, or VTOL; Low altitude, short-duration experiment; long endurance, Low altitude (LALE); middle altitude, long endurance: MALE; long endurance, high altitude (HALE) [8].

A vertical take-off and landing unmanned aerial vehicle is a part of the vertical take-off and landing unmanned aerial system, specifically designed for lifting heavy loads in difficult terrains.. These aircraft are mostly preferred due to the limitations of the terrain because it requires no take-off, or landing area [9]. They operate at different altitudes depending on their missions but are typically used for low-altitude flights. The high power consumption required for vertical hovering and flight reduces the flight time of a VTOL UAV. However, larger VTOL UAVs, which have enhanced lifting capabilities, can achieve longer flight durations [10]. This study focused on manufacturing a lightweight, high-strength VTOL UAV arm which is proper for rapid and mass production. Recently, carbon fibre frames with Al alloy connectors are frequently used for small-sized VTOL UAVs and are common in the market. For small-size UAVs, it is possible to increase the benefit-cost ratio for manufacturing a carbon fibre structure. Except for Mid-size and bigger-size UAVs, carbon fibre is not the first option because of manufacturing costs and limited machinability. In addition, carbon fibre frames are less suitable for mass production, modification and welding. On the other

*Corresponding author's e-mail: fatihakkoyunphd@gmail.com

hand, Aluminum (Al) is a lightweight material widely used in industry due to its high strength capability at low density. The average density of aluminum alloys is around 270 kg/m³. While 7000 series aluminum alloys offer a yield strength of approximately 540 MPa, they have poor weldability. In contrast, 6000 series aluminum alloys are preferred because they can be welded and have a yield strength comparable to that of low-carbon steel. To increase the flight duration and lifting capability of a UAV, there are two dominant parameters that should be considered. The first one is using lightweight structures with high-strength materials the other one is increasing the thrust it. For this purpose, in a study aluminum ASM 7075 material was used to optimize the weight of landing gears for aerial vehicles [12, 13]. Were focused on the thrust generated by a propeller for lifting heavy loads. A study conducted by [12] investigated a design method to reduce the weight of a structure during the manufacturing stage. A mini-UAV was developed and tested by Bronz, M. et.al. [13]. For providing thrust up to 6N using a mini-UAV. In a study conducted by LI, DUAN, & LIN in 2018, the significance of developing lightweight yet strong structures in modern aviation technology and mechanical design is highlighted. Specifically, the researchers focused on the design and development of a torque arm, emphasizing the importance of balancing weight reduction with maintaining high structural strength [14, 15].

The key challenges in designing and manufacturing the UAV arm included selecting materials for optimal weight and strength, as well as ensuring precision in fabrication and system integration. These challenges were addressed through advanced material choices, stress analysis, precision manufacturing techniques, and modular design for durability and cost management. The objective of this study was to design a mid-size VTOL UAV arm capable of generating high thrust for lifting heavy loads. To achieve the lack of a low-cost arm of a UAV, well-structured and lightweight high-strength aluminum materials were used in the prototyping stage of the arm. The prototyping process was conducted by focusing on the feasibility of rapid and mass production. The arm was designed using computer modelling software in 3D and structural analyses were conducted using the finite element analysis (FEA) method. A low-cost arm, a well-structured and lightweight prototype was created using aluminum materials known for their strength. For the relationship between thrust force and strain, an experimental test was conducted using a UAV arm testing mechanism. The arm was equipped with a brushless direct current (BLDC) motor and gear reducers, controlled by an electronic speed controller (ESC), to generate thrust. The study aimed to contribute to the development of more efficient and cost-effective UAV arms capable of handling heavier payloads by studying the performance and capabilities of the prototype arm. This study introduces a novel approach to the design and manufacturing of a mid-size VTOL UAV arm, focusing on the use of aluminum alloys to achieve a lightweight yet high-strength structure suitable for rapid and mass production. While previous research has explored carbon fiber structures for small UAVs, this study differentiates itself by concentrating on the use of aluminium in the context of larger UAVs, where the carbon fiber becomes less cost-effective and harder to work with [16]. Additionally, the study contributes to the field by optimizing the arm's structure for both lifting capacity and thrust generation, utilizing Finite Element Analysis (FEA) to verify the design's integrity. Unlike other studies that predominantly focus on propulsion or lightweight material choices, our work bridges these areas by creating a cost-efficient, mass-producible arm that enhances UAV performance in terms of payload capacity and endurance. This approach directly addresses the gap in the availability of affordable yet high-performing UAV components, making it a valuable contribution to both industrial and military UAV applications.

This study presents a novel design and manufacturing approach for a mid-size VTOL UAV arm, focusing on the use of aluminum alloys to achieve a lightweight, high-strength structure suitable for rapid and mass production. The aluminum arm was optimized for both lifting capacity and thrust generation, utilizing Finite Element Analysis (FEA) to ensure structural integrity. The study fills a gap in the UAV industry by offering a cost-efficient and high-performing alternative to carbon fiber for larger UAVs. The prototype was tested with a brushless motor and electronic speed controller to evaluate its thrust capabilities, contributing to advancements in UAV payload handling and endurance for both industrial and military applications [20].

2. EXPERIMENTAL

In this study, aluminum alloys were used to compose the arm of the VTOL UAV. These alloys are lightweight and common in the market in an industry that provides high strength with low density. The average density of aluminum alloys is around 270 kg/m³. The 7000 series aluminum alloys have yield strength of approximately 540 MPa but suffer from poor weldability. In contrast, 6000 series aluminum alloys are preferred for their weldability and yield strength, which is comparable to that of low-carbon steel.

Table 1. Comparison of materials, *E*, young's modulus; UTS, ultimate tensile strength; A_t (%); *ρ*, density; M., machinability; Test, test standard.

Material	*E (GPa)*	*UTS (MPa)*	*ρ (kg/m³)*	*M.*	*Test*
Carbon fiber T700S	150	2550	157	Low	ASTM D-3039
Alloy steel AISI 5130	205	1275	783	High	ASTM A752
Aluminum alloy 7075-T6	71.7	572	281	High	ASTM G-47

Comparison between aluminum, carbon fiber and steel shows high-strength forms of these materials. Comparison of mechanical properties for the elastic modulus, the tensile strength, machinability and density are shown in Table 1. The properties of materials are given in Table 1 for room temperature conditions. Environmental conditions such as temperature and humidity have a huge effect on carbon fiber composites as when this type of composite subjected the temperatures above 65 Cº properties will be reduced. And even more high humidity with heat will reduce the properties of these materials. But for metals like aluminum and steel, the properties will be close at these temperatures. For an aerial vehicle structure, the stiffness of the material is an important parameter because high strength is needed for this type of application but also it is not enough alone. A lighter material

with high strength is needed to achieve long flight duration with manoeuvrability [17, 18]. It is seen from Table 1 that carbon fiber is the lowest-density material and has remarkably high stiffness. However, these are unidirectional results for a laminate of carbon fiber. Typically, to increase the strength of a carbon fiber structure it needs to be layered in multiple directions. And if carbon fiber is layered in many directions to have the most uniform properties it ends up with very high strength properties close to aluminum, but it will be heavier than aluminum. For multidirectional structures, aluminum is a preferable option because of its lightweight and machinability with high strength [18].

A lightweight, well-structured, and high-strength aluminum arm was designed, produced, and tested for VTOL UAVs. It is aimed to produce a prototype that is proper for rapid manufacturing using conventional manufacturing techniques. In line with this direction, the prototyping process was conducted using widely used manufacturing techniques that are suitable for rapid and mass production. The chassis was designed in 3D using computer aided design (CAD) software and the finite element analysis (FEA) was realized using an engineering simulation environment. computer aided manufacturing (CAM) method was used to produce the main parts of the chassis and arm. The designed arm and its main shaft bearing are shown in Figure 1.

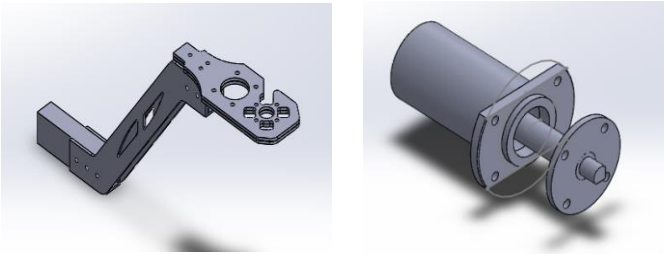

(a) (b)

Fig. 1. Computer model of (a) the arm, and (b) main shaft bearing.

The designed VTOL UAV arm shown in Figure 2 was constructed using Al 6068-T6 sheets, Al 6063-T6 rectangular weldment profile tubes, a gear reductor, and assembling parts made from Al 7075-T6. The arm weighs close to 1.0 kg as in Figure 3, which is comparable to the weight of carbon fiber arms available on the market. Unlike carbon fiber arms, it is appropriate for large-scale manufacturing., weldable, more affordable, and can be easily modified.

Fig. 2. Side view of the VTOL UAV arm.

Fig. 3. Gear reducer assembly and propeller on it.

A gear reducer in Figure 3 was used on the arm that consisted of helical gears with a ratio of 20/68. It was composed of a hardened steel pinion gear and a Delrin main gear. Aluminium parts were machined by laser cutting and assembled on a rectangle weldment profile. The propeller's main shaft, bearing house and connectors were lathe machined for the main shaft Al 7075 T6 material was used in Figure 3. Carbon fiber propellers were mounted on the gear reducers' main shaft. A 6.5 kW power BLDC motor and the gear reducer mounted on a motor holder. To drive the BLDC motor, a 160 A 59 V ESC was used. It was driven by a pulse width modulation (PWM) signal that is generated by a function generator. The ESC calibration was done by using the function generator for 100 Hz. The modulated signal was monitored and corrected with a logic analyzer. The ESC, a power switch, a spark switch and a 10S Li-Po battery were connected.

The thrust produced by a propeller depends on several factors, including air density, the propeller's RPM, its diameter, the shape and area of the blades, and its pitch. Since propellers with the same diameter and pitch frequently have different blade forms, areas, and flexibility depending on the brand and kind, accurately calculating the thrust is difficult. A propeller creates thrust at its base to move itself forward by converting the rotating motion from a power source into a fluid stream. The blades on a propeller are like revolving aerofoils that generate lift and drag. Their performance is directly tied to the propeller's blade function. Typically, propellers have two to six blades that are twisted to enhance efficiency. Lift refers to the net force perpendicular to the flow direction, while drag refers to the net force along the flow direction. The force generated on the blade surface by the propeller's rotation is the sum of lift and drag forces. When considering a spinning propeller blade as an actuator disc in Figure 4, the surrounding fluid passes through this disc, which acts as a plane where pressure changes can be studied. A propeller mounted on a rotor performs work on the airflow, creating a noticeable pressure difference across the propeller disc. This actuator disc can be used as a model to investigate these pressure changes.

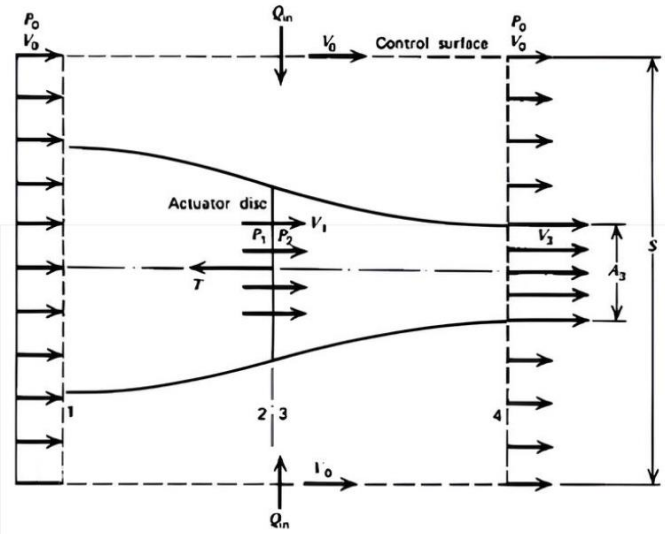

Fig. 4. Schematic of a propeller propulsion system (McCormick, 1979).

Thrust, as defined by the simple momentum theory, is the actuator disk's perpendicular force; it is calculated by multiplying the area of the propeller disc by the pressure jumps across the disc. The thrust force equation Equation (1) illustrates how propellers produce thrust through these pressure changes.

$$Thrust = F = \Delta p \cdot A \tag{1}$$

The pressure change, Δp, and the propeller disc area, A, are connected to the thrust produced by the propeller disc, represented as F. Every point on the propeller surface is affected by the mechanical forces brought about by the pressure jump, which are orientated perpendicular to the surface. By integrating the force fluctuations across the propeller blades' whole surface, the net force may be determined. Pressure varies at each point on the propeller surface due to the moving fluid, and this variation is related to the velocity of the fluid. To determine the net force, the pressure distribution can be calculated using Bernoulli's equation, which relates pressure and velocity. When the fluid velocity is low and external energy effects are negligible, Bernoulli's equation can be applied to express the relationship between pressure and velocity. Assuming an ideal fluid and disregarding boundary layers, the propeller surface can be considered a streamline. As indicated in Figure 4, the total pressure in front of the disk, (pt0), is the sum of the static pressure, (p0), and the dynamic pressure, (pd).

A pressure difference is;

$$\Delta p = pt_e - pt_0 \tag{2}$$

where Δp; pressure difference, pt_e; inlet pressure, pt_o; outlet pressure

$$pt_e = p_0 + p_d \tag{3}$$

$$pt_0 = p_0 + p_d \tag{4}$$

$$p_d = \frac{1}{2}\rho v^2 \tag{5}$$

From the equations indicated in Equations (2-5), the force-pressure relationship can be expressed as indicated in Equations (6) and (7).

$$\Delta p = \frac{1}{2}\rho \cdot (V_e^2 - V_0^2) \tag{6}$$

$$F = \frac{1}{2}\rho \cdot A \cdot (V_e^2 - V_0^2) \tag{7}$$

where Δp: dynamic pressure (N/m^2), ρ: density of fluid (kg/m^3) and v: velocity (m/s).

In addition to these theoretical definitions, the net force on a propeller's body is caused by pressure differences across its surface. This net mechanical force can be calculated by dividing the propeller's surface into a large number of small sections and then integrating the forces over the whole surface in Equation (8).

$$F = \sum_{surface} \underset{p}{\rightarrow} \cdot \Delta A = \oint \underset{p}{\rightarrow} \cdot dA \tag{8}$$

A propeller increases air density as it flows through the propeller disc area, idealized as a stream tube passing through the disc. This is explained by the momentum theory, or disk actuator theory, which models the propeller as an ideal actuator disk. According to this theory, there is no energy lost to frictional drag since the flow is assumed to be inviscid and steady, or ideal flow. The rotor functions as an actuator disc with an unlimited number of blades with an infinite aspect ratio, producing thrust without inducing rotation in the slipstream. The thrust equation Equation (9) states that the mass flow rate through the propeller and the velocity change the propulsion system imparts are what determine thrust.

$$T_{theory} = \rho \frac{\pi d^2}{4}\, x\, \frac{p^2}{3600}\, \omega_{RPM}^2 \tag{9}$$

where: T: theoretical thrust (N), ρ=1.225kg/m^3, p: diameter (m), d: pitch (m), ω_{RPM}^2: angular velocity (rpm) [19].

In general, a propeller's length increases power but also raises motor heating, while its pitch allows for higher RPM but results in higher current draw. Reducing the propeller's pitch or length is an effective way to address heat issues, though this limits the vehicle's performance. To select the optimal pitch, parameters like propeller rotational limitations, power consumption, ideal speed, and gear reduction need to be considered. Performance data for the propeller are evaluated using a thrust test apparatus, as shown in Figure 5, to measure power consumption, thrust, and angular velocity. To evaluate performance, the outcomes of the test mechanism are compared with calculations made theoretically. A fixed cantilever mechanism was used to investigate the VTOL UAV arm thrust and strain relationship. A 3D model of the test mechanism is shown in Figure 5.

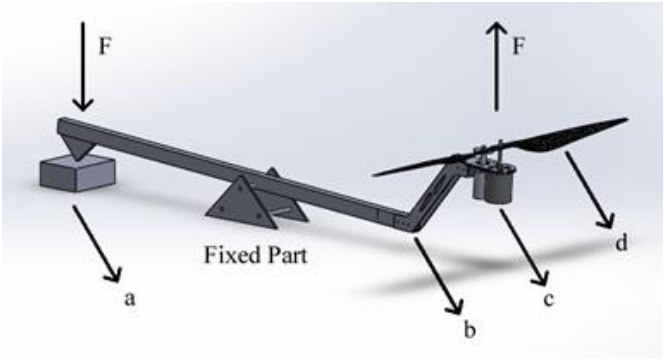

Fig. 5. The computer model of the test mechanism; (a) Precision scale, (b) Junction of the chassis and arm c) BLDC motor and gear reducer with motor holder, d) The propeller.

A force transducer, which converts force into an electrical signal, was used to measure strain variations. These transducers typically include strain gauges arranged in a wheatstone bridge configuration and are commonly employed in industrial applications to sense loads. In this step, a force transducer and measurement system were utilized to assess force variations on the VTOL UAV arm. Figure 6 illustrates the layout of the strain gauges on the UAV arm. The arm is mounted on a cantilever mechanism for investigating the shear strain and thrust relationship. To measure shear strain, quarter bridges and rosette-type strain gauge layouts are used on the arm of the UAV. 5V excitation voltage was applied for supplying bridges and the resistance of each strain gauge was 360 Ω with gain factor (GF) two.

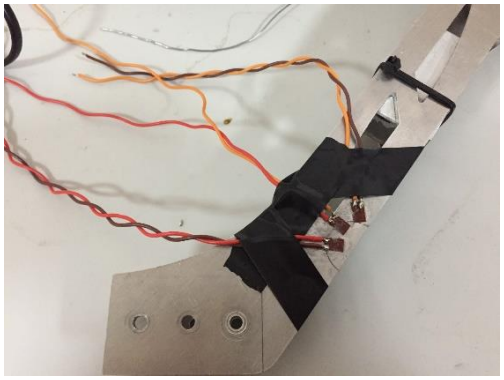

Fig. 6. Quarter bridge strain gauge circuit and rosette type layout.

Resistance of a material depends on the material type and volume of the material Equation (10).

$$R = \frac{\rho \cdot L}{S} \tag{10}$$

Where: R: resistance, ρ: resistivity, L: length, S: cross-sectional area.

By calculating the resistance differential, strain variations can be determined Equation (11).

$$\Delta R = GF \cdot \epsilon \cdot R \tag{11}$$

where: ΔR: Resistance difference, GF: Gage factor, Є: Strain, R: Resistance.

The wheatstone bridge, which measures voltage differential, can be used to evaluate the output Equation (12).

$$Vo = Vex\left[\frac{R_1}{R_1+R_2} - \frac{R_3}{R_3+R_G}\right] \tag{12}$$

The block diagram of the strain measurement system is shown in Figure 7.

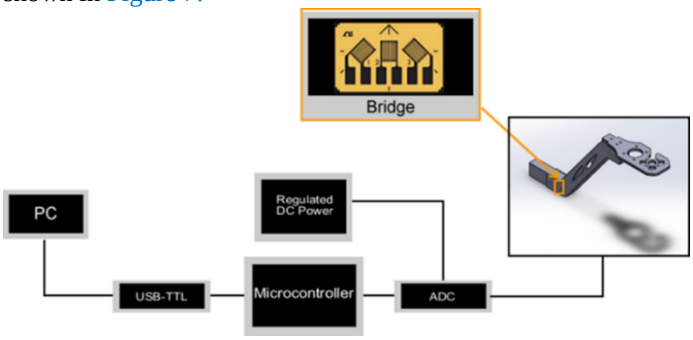

Fig. 7. Block diagram of the strain measurement system.

The Wheatstone bridge on the VTOL UAV arm was powered by regulated DC sources to collect strain values from the arm. The analogue signals generated by the bridge were acquired using 24-bit ADCs, which converted the signals to digital form. The digital data was then transmitted to a computer over serial communication through a microcontroller unit. A regulated DC source was used to feed the bridge, and cable shields were connected to the ground. A Rosette-type strain gauge was used to measure shear strain on the arm. Regulated DC power sources were utilized to feed the bridge on the VTOL UAV arm to measure strain variations from the arm. The bridges' analogue output was transformed to digital using 24-bit ADCs. An ADC digitizes signals, and a microcontroller uses serial transmission to send the output to a PC. The Wheatstone bridge is powered by a regulated DC power source, which reduces noise levels as in Figure 8.

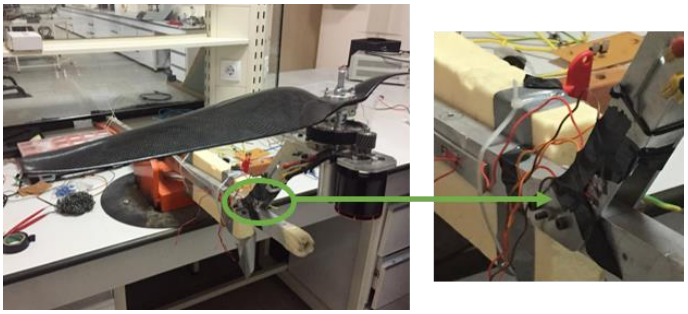

Fig. 8. The Wheatstone bridge on the VTOL UAV arm.

To convert the digital outputs of the ADC from digital value to voltage value formulas Equation (13-15) are used.

$$Vin = ADC\ Digital\ Output\ x\ ADC\ Step\ Response \tag{13}$$

where, Vin: ADC input voltage, LSB: Least Significant Bit

$$ADC\ Step\ Response\left(\frac{V}{digital\ output}\right) = \frac{FSR}{2^n} \tag{14}$$

$$FSR = \frac{Vex}{Gain} \tag{15}$$

The voltage-to-strain relationship can be determined with the Wheatstone bridge formula as shown in the formula Equation (16 and 17).

$$\Delta R4 = R + (R3 - (\frac{R3}{\frac{R1}{R1+R2} - \frac{Vo}{Vin}}) \quad (16)$$

$$\varepsilon = \frac{\Delta R}{GFxR} \quad (17)$$

For determining factor and offset values for each gage measurements were recorded repetitively via serial communication by a computer. The acquired experimental strain results are presented in Figure 9 as *Ea*, *Eb*, and *Eab*, respectively.

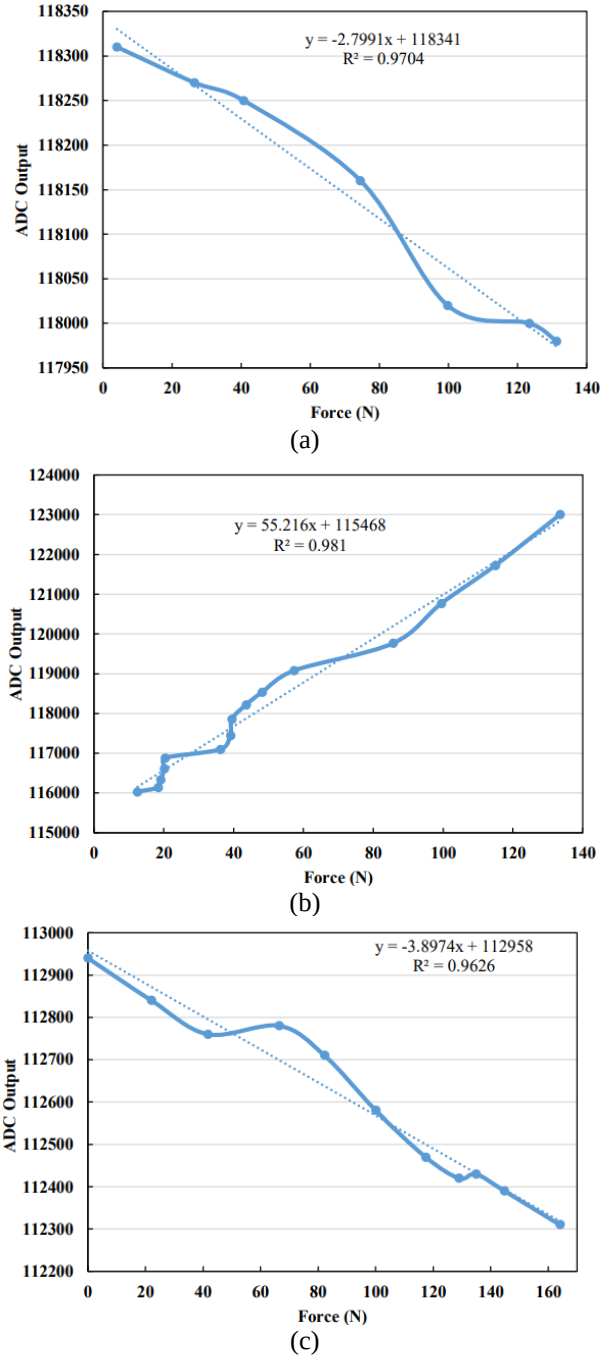

Fig. 9. Strain on; a) X-axis (*Ea*), b) Y-axis (*Eb*), and c) XY-axis (*Eab*).

The average results derived from the slope formula based on the strain measurements are; Avg (Єa) = -21.7111, Avg (Єb) = -17.0539, and Avg (Єc) = 11.6556.

The coordinate transformation equation is denoted in Equation (18) was used to calculate the plane and shear strain observed on the arm.

$$\varepsilon_a = \frac{\varepsilon_x + \varepsilon_y}{2} + \frac{\varepsilon_x - \varepsilon_y}{2} cos2a + \varepsilon_{xy} sin2a$$

$$\varepsilon_b = \frac{\varepsilon_x + \varepsilon_y}{2} + \frac{\varepsilon_x - \varepsilon_y}{2} cos2(a+\beta) + \varepsilon_{xy} sin2(a+\beta)$$

$$\varepsilon_c = \frac{\varepsilon_x + \varepsilon_y}{2} + \frac{\varepsilon_x - \varepsilon_y}{2} cos2(a+\beta+y) + \varepsilon_{xy} sin2(a+\beta+y) \quad (18)$$

3. RESULTS

Al 6063-T6 rectangular weldment profile tubes, Al 6068-T6 sheets, and Al 7075-T6 gear reducer and connector pieces were used in the construction of the VTOL UAV arm. The arm weighs 1.0 kg, which is about the same as commercially available carbon fibre arms. Compared to carbon fibre arms, it is more inexpensive, easier to modify, appropriate for mass production, and weldable. Figure 10 displays the Von-Mises stress findings for the UAV arm. On the arm, the maximum stress in Figure 10 (a) is $5.455 \times 10^{+7}$ N/mm^2, and the maximum strain in Figure 10 (b) is 4.500×10^{-4}. The value of the factor of safety (FoS) in Figure 10 (c) is 4.94. The displacement maximum value in Figure 10 (d) is 2.246 mm.

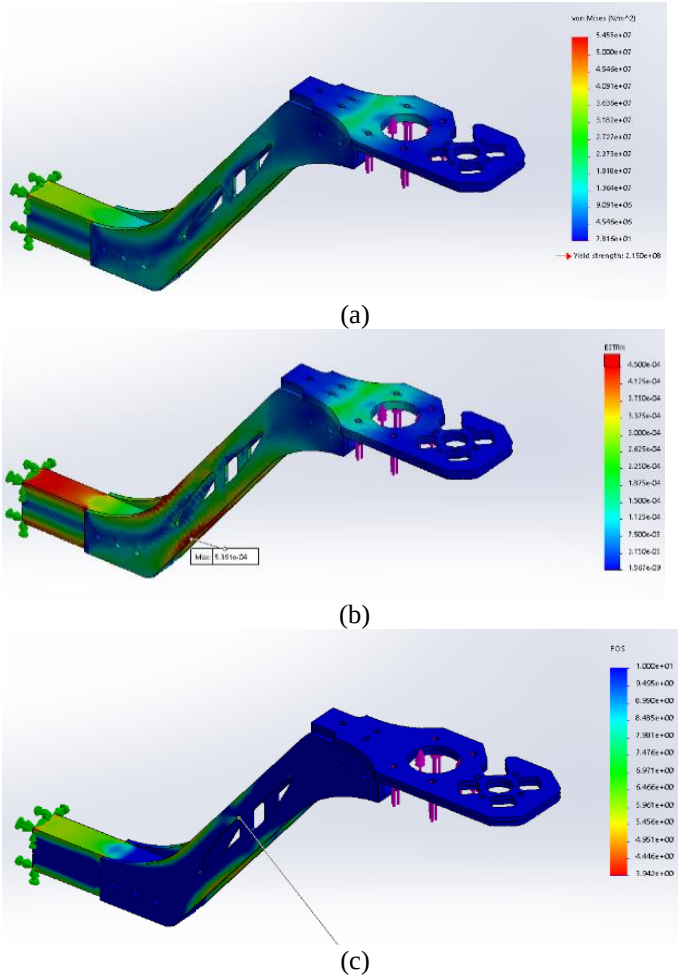

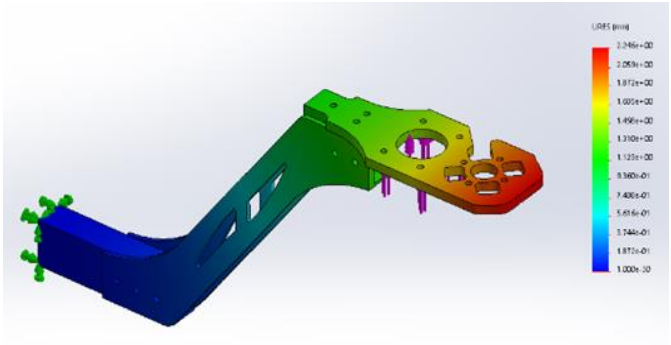

(d)

Fig. 10. VTOL UAV Arm; (a) Stress, (b) Strain, (c) FoS and (d) displacement analysis results.

Using a strain measuring setup and a Rosette-type strain gauge, the strain on the VTOL UAV arm induced by the propeller thrust force was examined. The link between voltage and strain was computed theoretically. The VTOL UAV arm's finite element analysis (FEA) strain results were compared to experimental strain results. Using the theoretical theory, the force and voltage relationship was determined. The resistance of the strain gauge was 360 Ω, and the gain factor was two.

The static structural analysis simulation results present data on various strain measurements under applied forces. The applied force in Newtons and the corresponding principal strain indicates the maximum strain experienced by the material. It also provides measurements of shear strain in the XY, XZ, and YZ planes, as well as normal strains in the X and Y directions. This comprehensive dataset allows for an in-depth analysis of how different forces impact the material, revealing insights into the material's performance and structural integrity under static load conditions.

The comparison between the experimental results for the principal strain (SN1) and the analysis results (principal strain) is shown in Figure 11. The results exhibit a slight difference, indicating that they are very close to each other, which is satisfactory.

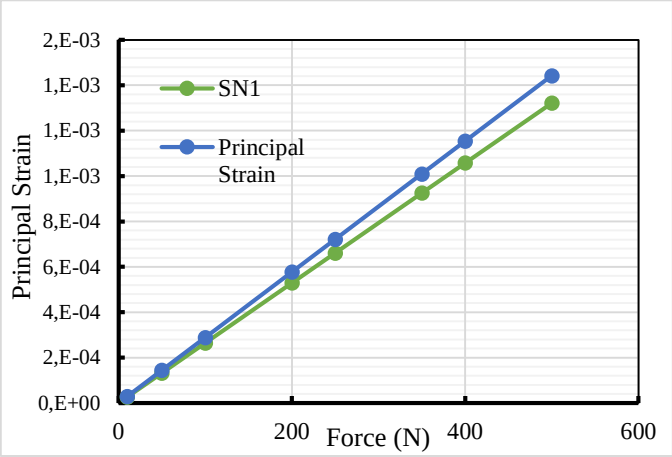

Fig. 11. Principal strain comparison.

The comparison between the experimental results for shear strain (ϵ_{xy}) and the analysis results (shear strain) is presented in Figure 12. The results demonstrate a clear correspondence between theoretical predictions and experimental observations.

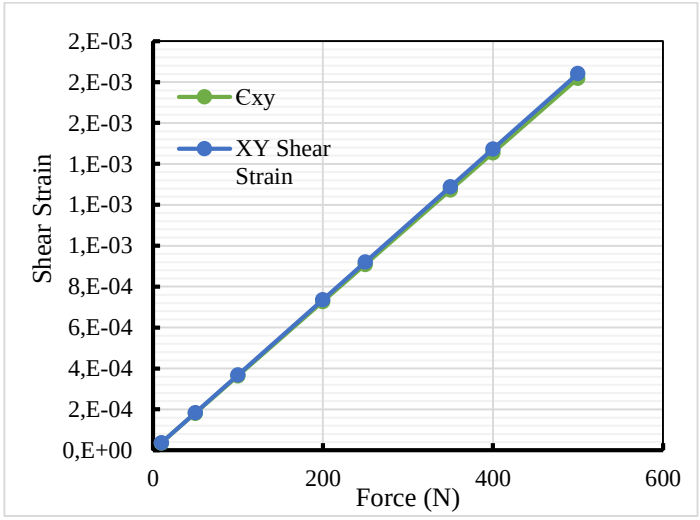

Fig. 12. Shear strain comparison.

The comparison of power, thrust, and strain is detailed in the table, which includes measurements of X, Y, and XY strains. The result provides a comprehensive analysis of how variations in power and thrust impact the strain on the VTOL UAV arm. Specifically, it shows how each component of strain on the X axis (representing longitudinal strain), the Y axis (representing latitudinal strain), and the XY plane responds to different levels of power and thrust. This comparison helps in understanding the relationship between the operational parameters of the UAV and the resulting structural stresses on the arm, providing valuable insights for optimizing performance and ensuring structural integrity.

Figure 13 contrasts shear strain, a measure of material deformation under shear stress, with static thrust, which quantifies the force exerted in a stationary state. It highlights their different applications and implications in engineering contexts.

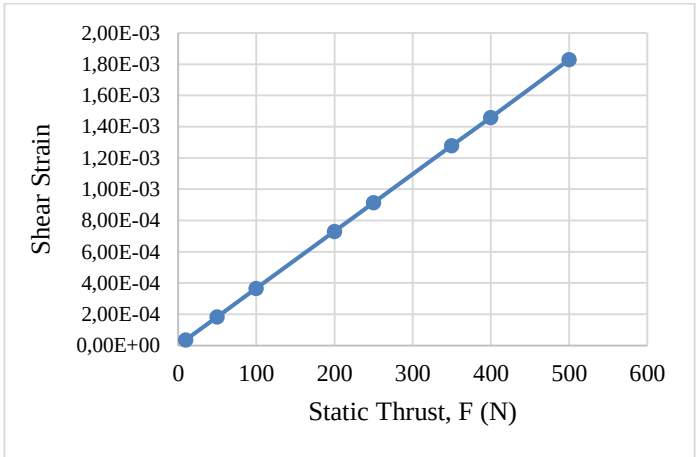

Fig. 13. Shear strain, static thrust comparison.

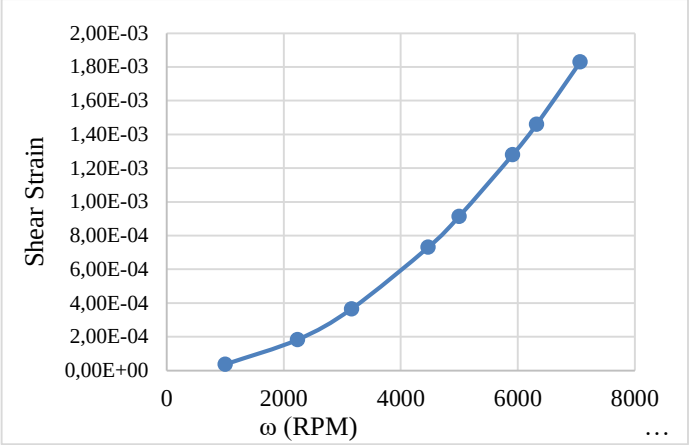

Fig. 14. Shear strain, angular velocity comparison.

For the developed arm, properties of carbon fiber, aluminum, and steel were assessed using FEA simulation software, with results summarized in Table 2. This table provides a comparison of the materials based on their FoS, weight in grams, and cost percentage. The FoS indicates the safety margin each material offers under load, while the weight and cost columns highlight the practical considerations of using each material for the VTOL UAV arm.

Table 2. Electronic components are used for strain measurement [17, 18].

Material	*FoS*	*Weigth (g)*	*Cost (%)*
Carbon fiber T700S	5	750	300
Alloy steel AISI 5130	4	3000	100
Aluminum alloy 6068-T6	5	1000	120

4. CONCLUSION

In this study, the design and development of a high-strength, lightweight arm for VTOL UAVs was successfully achieved. The findings demonstrate that thermally processed aluminum is an effective material for UAV arms when weight and strength are key considerations. While carbon fiber offers superior strength and lower weight, it is more effective in handling one-dimensional forces and presents challenges in welding and machinability. In contrast, aluminum provides a more practical solution for multidimensional forces, offering both weldability and machinability. Tempered aluminum, in particular, proved to be a cost-effective and modifiable material for mid-size UAV arm production.

The arm was designed as a hybrid structure, combining aluminum alloy with carbon fiber composites. This allowed for optimal weight reduction while maintaining the necessary strength for UAV operations. Precision machining processes were used for manufacturing without the need for welding, showcasing the material's flexibility. The performance of the arm was validated through static load testing, confirming its strength and durability under demanding conditions. In summary, this study highlights the benefits of using thermally processed aluminum in UAV arm manufacturing, offering a cost-effective, modifiable, and high-performing solution suitable for VTOL UAV applications.

Acknowledgement

This work was supported by the Adnan Menderes University Project No: MF17013-20202. The authors would like to express their sincere thanks to Adnan Menderes University for their financial support and contributions to this research.

References

[1] M. H. Sabour, P. Jafary, and S. Nematiyan, "Applications and classifications of unmanned aerial vehicles: A literature review with focus on multi-rotors," *The Aeronautical Journal*, 127(1309), pp. 466–490, 2023.

[2] J. del Cerro, C. C. Ulloa, A. Barrientos, and J. de León Rivas, "Unmanned Aerial Vehicles in Agriculture: A Survey," *Agronomy*, 11(2), pp. 203, 2021.

[3] S. A. H. Mohsan, M. A. Khan, F. Noor, I. Ullah, and M. H. Alsharif, "Towards the Unmanned Aerial Vehicles (UAVs): A Comprehensive Review," *Drones*, 6(6), pp.147, 2022.

[4] B. Stark, B. Smith, and Y. Q. Chen, "A guide for selecting small unmanned aerial systems for research-centric applications," IFAC Proceedings Volumes, 46(30), pp. 38-45, 2013.

[5] H. Eisenbeiß, "UAV Photogrammetry," University of Technology Dresden, *PhD Thesis*, pp 0-237, 2009.

[6] S. Kedari, P. Lohagaonkar, M. Nimbokar, G. Palve, and P. P. Yevale, "Quadcopter - A Smarter Way of Pesticide Spraying," 2(6) pp. 1257–1260, 2016.

[7] R. K. Rangel, K. H. Kienitz, and M. P. Brandao, "Development of a multi-purpose portable electrical UAV system, fixed & rotative wing," *IEEE Aerospace Conference Proceedings*, 2011.

[8] M. H. Sabour, P. Jafary, and S. Nematiyan, "Applications and classifications of unmanned aerial vehicles: A literature review with focus on multi-rotors," *The Aeronautical Journal*, 127(1309), pp. 466–490, 2023.

[9] H. Yao, R. Qin, and X. Chen, "Unmanned Aerial Vehicle for Remote Sensing Applications—A Review," *Remote Sensing 2019*, 11(12), pp. 1443, 2019.

[10] J. del Cerro, C. C. Ulloa, A. Barrientos, and J. de León Rivas, "Unmanned Aerial Vehicles in Agriculture: A Survey," *Agronomy* 11(2), pp. 203, Jan. 2021.

[11] A. Satish, V. Ravi, and B. C. Shekar, "Topology optimization of landing gear's leg for aerıal vehıcle usıng ansys," 4(7), pp. 1046–1054, 2018.

[12] Y. L. Ma, J. R. Tan, D. L. Wang, and Z. Z. Liu, "Light-weight design method for force-performance-structure of complex structural part based co-operative optimization," *Chinese Journal of Mechanical Engineering (English Edition)*, 31(2), pp. 1-9, 2018.

[13] M. Bronz, E. J. J. Smeur, H. G. de Marina, and G. Hattenberger, "Development of a fixed-wing mini UAV with transitioning flight capability," *35th AIAA Applied Aerodynamics Conference*, 35(1) pp. 1-14, 2017.

[14] J. K. Li, F. F. Duan, and R. G. Lin, "Topology Optimization to Torque Arm in Landing Gear System Based on ANSYS Workbench," *DEStech Transactions on Engineering and Technology Research*, pp. 46–50, 2018.

[15] M. Tokatlı, E. Uslu, M. Çolak, Ç. Yüksel "Investigation of the effect of liquid metal quality on feedability in the casting of A356 aluminum alloys," *Turkish Journal of Electromechanics & Energy*, 7(3), pp.105-109, 2022.

[16] U. Topal, H. Can, "Development and critical design of magnetic torque rod for LEO satellites," *Turkish Journal of Electromechanics & Energy*, 9(1), pp.3-9, 2024.

[17] B. Sadeghi, P. Cavaliere, C. I. Pruncu, M. Balog, M. Marques de Castro, and R. Chahal, "Architectural design of advanced aluminum matrix composites: a review of recent developments," *Critical Reviews in Solid State and Materials Sciences*, 49(1), pp.1-71, 2024.

[18] L. Zhu, N. Li, and P. R. N. Childs, "Light-weighting in aerospace component and system design," *Propulsion and Power Research*, 7(2), pp.103-119, 2018.

[19] M. Yoon, "Experimental Identification of Thrust Dynamics for a Multi-R otor Helicopter," *International Journal of Engineering Research & Technology (IJERT)*, 4(11), pp. 206–209, 2015.

[20] F. Akkoyun, "Design and development of an unmanned aerial and ground vehicles for precision pesticide spraying," *PhD Thesis*, Aydın Andan Menderes University, Türkiye, 2019.

Biographies

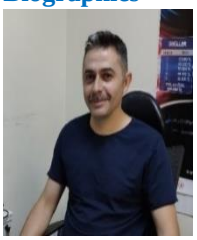

Fatih Akkoyun received his M.Sc. degree in Electronic and Computer Education from Kocaeli University in 2011 and his Ph.D. in Mechanical Engineering from Adnan Menderes University in 2020. He is currently an assistant professor in the Department of Mechanical Engineering at İzmir Demokrasi University. His research focuses on robotics, sensor technologies, and automation systems, with a particular emphasis on robotic control and sensor integration for industrial applications.

E-mail: fatih.akkoyun@adu.edu.tr

İsmail Böğrekci earned his M.Sc. degree in Mechanical Engineering from Cranfield University in 1996, followed by a Ph.D. in Mechanical Engineering from the same institution. He is currently a professor in the Department of Mechanical Engineering at Aydın Adnan Menderes University, where he has been a faculty member since 2009. His research interests are primarily focused on robotics, sensor systems, and automation. He has worked extensively on the design and development of advanced robotic systems, specializing in multi-robot coordination, sensor integration, and autonomous control for industrial and UAV applications. Prof. Bogrekci has published numerous papers in international journals and conferences, contributing significantly to the fields of robotics, sensors, and mechanical systems design. He is also actively involved in projects that bridge academia and industry, aiming to enhance robotic efficiency in real-world applications.

E-mail: ibogrekci@adu.edu.tr